ELSEVIER

Medical Engineering & Physics 24 (2002) 253–264

Medical Engineering & Physics

www.elsevier.com/locate/medengphy

Simulation of mechanical responses of fingertip to dynamic loading

J.Z. Wu *, R.G. Dong, S. Rakheja, A.W. Schopper

National Institute for Occupational Safety and Health, Morgantown, West Virginia 26505, USA

Received 8 October 2001; received in revised form 3 January 2002; accepted 28 January 2002

Abstract

Extended exposure to mechanical vibration has been related to many vascular, sensorineural and musculoskeletal disorders of the hand–arm system, frequently termed 'hand–arm vibration syndrome' (HAVS). A two-dimensional, nonlinear finite element model of a fingertip is developed to study the stress and strain fields of the soft tissue under dynamic loading, that may be encountered while grasping and operating a hand-held power tool. The model incorporates the most essential anatomical elements of a fingertip, such as soft tissue, bone, and nail. The finger is assumed to be in contact with a steel plate, simulating the interaction between the fingertip and a vibrating machine tool or handle. The soft tissue is assumed to be nonlinearly visco-elastic, while the nail, bone, and steel plate are considered to be linearly elastic. In order to study the time-dependent deformation behavior of the fingertip, the numerical simulations were performed under ramp-like loading with different ramping periods and sinusoidal vibrations of the contacting plate at three different frequencies (1, 10, and 31.5 Hz). Owing to relatively large deformations of the soft tissue under specified static and dynamic loading, Lagrangian large deformation theory was applied in the present analysis. The effects of the loading rate and the frequency of the sinusoidal vibration on the time-dependent strain/stress distributions in the different depth within the soft tissue of the fingertip are investigated numerically. Our simulations suggest that the soft tissue of the fingertip experiences high local stress and strain under dynamic loading and the fingertip may separate from the vibrating contact surface due to the viscous deformation behaviour of the soft tissue. For a given deformation, the high frequency loading produces a higher stress in the tissues compared to that obtained at a low frequency loading. The present model may serve as a useful tool to study the mechanism of tissue degeneration under vibratory loading encountered during operation of hand-held power tools. Published by Elsevier Science Ltd on behalf of IPEM.

Keywords: Hyperelastic; Finite element analysis; Soft tissue mechanics; Vibration; Visco-elastic

1. Introduction

It is accepted that an extended exposure to mechanical vibration can induce an array of vascular, sensorineural and musculoskeletal disorders of the hand and arm of the operators. Such disorders are collectively termed the 'hand–arm vibration syndrome' (HAVS) [1–3]. The severe health risks posed by prolonged occupational exposure to power hand tool vibration, supported by findings of the epidemiological studies [4,5], have prompted several theoretical and experimental studies to enhance an understanding of the injury mechanisms. These studies have focused on the characterization of vibration amplitude and power flow in the coupled hand, tool and work piece system, the potential performance benefit analysis of vibration attenuation mechanisms, and the development of measurement methods and test rigs for assessment of vibration transmission of different tools.

Mechanical equivalent models of the human hand and arm have been developed to characterize its response to vibration on the basis of measured driving-point mechanical impedance [6,7]. The majority of the previous models are comprised of lumped mass, stiffness and damping elements, where the lumped parameter values are determined upon fitting curves to the data measured within a specified range of test conditions. Thus, they do not adequately represent the biomechanical properties of the human hand and arm. For example, the reported models characterize the biodynamic behaviour of the hand and arm under uncoupled vibration along the three

* Corresponding author. E&CTB/NIOSH/CDC, 1095 Willowdale Road, MS 2027, Morgantown, WV 26505, USA, Tel.: +1-304-285-5832; fax: +1-304-285-6265.

E-mail address: jwu@cdc.gov (J.Z. Wu).

1350-4533/02/$22.00 Published by Elsevier Science Ltd on behalf of IPEM.
PII: S1350-4533(02)00018-8

orthogonal axes defined in ISO-8727 [8], where the coupling effects were neglected. Although these models have served as important tools to study effects of direction and magnitude of vibration on the 'hand-transmitted vibration' (HTV) [9,10], they have provided little insight into the potential injury mechanisms and the pathological changes in the biological tissues caused by HTV.

A few studies have speculated on a potential injury mechanism leading to the onset of vibration induced white finger (VWF) disease [11,12]. The occurrence of VWF among exposed workers has been related to impaired blood circulation in the fingers resulting in degeneration of the vascular system, termed Raynaud's phenomenon of occupational origin [4] and traumatic vasospastic disease (TVD) [13,14]. It has been suggested that the occurrence of high contact pressures at the tips of the index and middle fingers under tool vibration affects the hemodynamic forces in the arterial walls and produces alterations to the arterial blood flow to the finger tips [15–17]. Gemne and Pyykko [5] suggested the concept of the growth of the muscle layer in the vessel wall caused by repeated contraction, thereby reducing the flow of blood in the vessels. The hypothesis is further supported by evidence of the onset of VWF disease at the tips of index, middle, and ring fingers [18,19], and the occurrence of the high grip pressure at the hand–handle interface [20]. Owing to the technical complexities associated with efforts to measure the interface pressure and the blood flow under vibration conditions and to characterize soft tissue in the fingertips, no attempts have been made to establish a correlation between the interface pressure and arterial blood flow.

Skin and soft tissue play predominant roles in the interactions between hand and power tools, and the 'to-the-hand' and 'through-the-hand–arm' transmission of the vibration energy. Owing to the highly nonlinear elastic and viscoelastic properties of the skin and soft tissues in the finger, the reported biodynamic models composed of linear springs, damping, and mass elements could not be applied to model biodynamic behaviour of the skin and soft tissues. A study of the time-dependent response of finger skin and soft tissue to localized, dynamic contact pressure could yield considerable insight into the mechanisms leading to tissue and arterial loading, and potentially, the impairment of finger blood flow. Such an analysis, however, would necessitate the knowledge of time-dependent stress and deformation fields within the soft tissue during vibration and knowledge of the localized dynamic contact pressure at the interface of the hand and the power tool handle. The mechanical properties of skin and soft tissue have been investigated extensively in vitro and in vivo using extensometers [21,22] or ultrasonic techniques [23]. It is generally accepted that skin and soft tissue are nonlinearly elastic [24], characterized by a low-stiffness region at small strains followed by a dramatic increase in stiffness as the strain is increased. Moreover, the mechanical properties of skin and soft tissue have been identified as time-dependent, i.e. they are visco-elastic [25]. The viscoelasticity of skin and soft tissue has been investigated by many researchers, in vivo, using a stress relaxation protocol [26,27]. In such a test, a step load (typically tension) is applied to the specimen and the resulting static displacement of the specimen is held constant by varying the applied force, until a steady state is reached. For skin, typically, it has been observed that 20–50% of the initially applied load can be recovered during a relaxation period of 30–80 s [27–29].

High concentration of the interface pressure at the fingertip, which occurs while operating a hand-held machine, can apply excessive loading on the skin and soft tissues, which could introduce excessive deformation of arterial walls, and thus interfere with normal blood flow in the fingertips. The deformation of the arterial vessels is speculated to be associated with the stress and strain fields within the soft tissue. The purpose of the present research is to develop a model based on finite element techniques to simulate the mechanical responses of a fingertip to dynamic loading and the stress/strain distributions in the soft tissue in the vibration environment. The model is two-dimensional and incorporates the essential anatomical structures of a finger: soft tissue (representing both the skin and the subcutaneous tissues), bone, and nail. The finger is assumed to be in contact with a steel plate, simulating the interaction between hand and a vibrating machine tool or handle. The soft tissue is assumed to be nonlinearly elastic and linearly viscoelastic; the nail, bone, and steel plate were considered as linearly elastic. The mechanical characteristics of all biological materials in the model were identified from the experimental data reported in the literature.

2. Methods

2.1. Constitutive equation of soft tissue

The soft tissue is assumed to experience large deformation; and possess nonlinearly elastic and linearly viscoelastic properties. The total tissue stress (Cauchy stress), $\sigma_{ij}(t)$, is assumed to be decomposed into an elastic stress, $\sigma^{0}_{ij}(t)$, and a viscous stress, $\sigma^{v}_{ij}(t)$. The elastic stress is associated with the long term material behaviour; while the viscous stress reflects the time-dependent characteristics of the tissue. The constitutive relations for such nonlinear elastic and linearly viscoelastic materials are expressed as [30]:

$$\sigma_{ij}(t) = \sigma_{ij}^{0}(t) + \sigma_{ij}^{v}(t)$$
$$\sigma_{ij}^{v}(t) = \int_0^t \dot{g}(\tau)\sigma_{ij}^{0}(t-\tau)\mathrm{d}\tau;\ i,j = 1,2,3 \quad (1)$$

where $\dot{g}(t)$ is the time-derivative of the the stress relaxation function, $g(t)$, which is defined using Prony series [31]:

$$g(t) = \left[1 - \sum_{i=1}^{N_G} g_i\left(1 - e^{-\frac{t}{\tau_i^G}}\right)\right] \quad (2)$$

where g_i and τ^G_i (i=1,2,$\cdots N_G$) are stress relaxation parameters; and N_G is the number of the series terms. It is assumed here that the stress relaxation behaviour in volumetric deformation is identical to that in the shear deformation.

Owing to the large deformation of the soft tissues under high localized loading, a finite deformation analysis is applied to the soft tissue in the present study. Elastic stress in the soft tissue (Cauchy stress), σ^0_{ij}, is determined by a constitutive equation [32]:

$$\sigma_{ij}^{0} = 2F_{ir}\frac{\partial(\rho_0 U)}{\partial C_{rs}}F_{sj};\ i,j = 1,2,3. \quad (3)$$

where F_{ij} and C_{ij} are the tensors of the deformation gradient and the right Cauchy–Green deformation, respectively; U is the strain energy per unit mass, ρ_0 is the mass density in undeformed state, so ($\rho_0 U$) is the strain energy per unit volume. In this study, we have adopted the strain energy function proposed by Storakers [33]:

$$\rho_0 U = \sum_{i=1}^{N}\frac{2\mu_i}{\alpha_i^2}\left[\lambda_1^{\alpha_i} + \lambda_2^{\alpha_i} + \lambda_3^{\alpha_i} - 3 + \frac{1}{\beta}((J)^{-\alpha_i\beta} - 1)\right] \quad (4)$$

where J=$\lambda_1\lambda_2\lambda_3$, with λ_i(i=1,2,3) being the principal stretch ratios, is the volume ratio; α_i and μ_i(i=1,$\cdots N$) are the exponential hardening parameters and generalized shear modulus, respectively; β=ν/(1−2ν) where ν is the Poisson's ratio; and N is the number of the terms needed to fit to the experimental data satisfactorily.

The material properties in Eq. (4) are determined by performing uniaxial or constrained tension/compression tests. The nominal stress in the stretch direction is expressed as [30]:

$$\sigma_j^0 = \frac{\partial(\rho_0 U)}{\partial\lambda_j} = \frac{2}{\lambda_j}\sum_{i=1}^{N}\frac{\mu_i}{\alpha_i}(\lambda_j^{\alpha_i} - J^{-\alpha_i\beta}) \quad (5)$$

where σ^0_j is the Cauchy stress in the direction of the stretch and λ_j(j=1,2,3) are the principal stretch ratios.

2.2. Finite element model

The dynamic interaction between a fingertip and steel plate is simulated using a two-dimensional finite element model (Fig. 1). The model is composed of linearly elastic bone and nail, and nonlinearly elastic and visco-elastic soft tissue, which is assumed to be in contact with a linearly elastic steel plate with a smooth surface. The contact between the skin surface and the steel plate is assumed to be frictionless. The bone within the fingertip was assumed to be fixed. The steel plate is subjected to a prescribed vertical displacement, $\Delta(t)$, simulating the vibration of the handle of a power tool (Fig. 1); $F(t)$ is the resultant contact force of the fingertip. The dimensions of the fingertip are assumed to be representative of the index finger of a male subject [34]. The cross section of the fingertip and the bone are assumed to be elliptical and the tissue thickness is considered to be asymmetric about the bone (Fig. 1). The tissue thickness between the bone and the skin surface contacting the steel plate is assumed to be larger than that between the bone and the nail, as shown in Fig. 1. The finite element model is developed using a commercial finite element software package Abaqus (version 5.8), and is composed of 421 eight-node, quadratic, plain-strain elements (Element type: CPE8).

The Young's moduli of the bone and nail are assumed as 17.0 GPa and 170.0 MPa, respectively, on the basis of the published experimental measurements [35], while Poisson's ratio is assumed to be 0.30 for both. The long

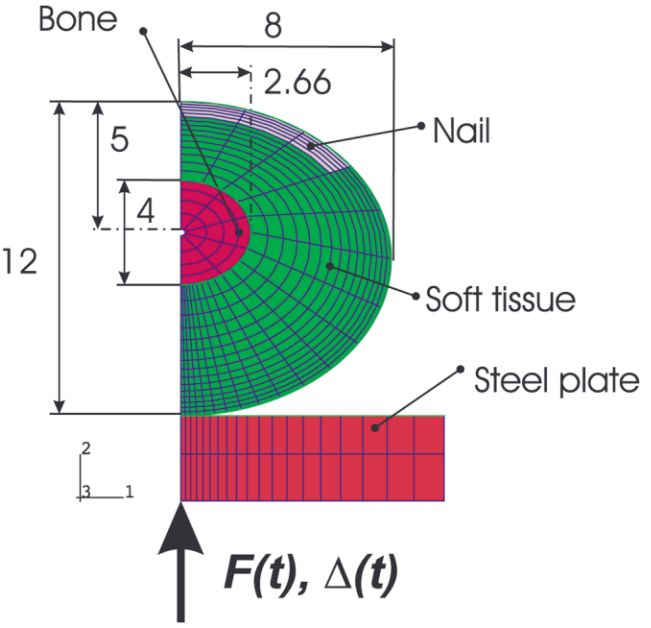

Fig. 1. Finite element model simulating the interaction between fingertip and vibratory power tool. The bone, nail, and steel plate are assumed to be linearly elastic; the soft tissue is assumed to be nonlinearly elastic and linearly viso-elastic. The model is composed of 421 eight-node, nonlinear, plain-strain elements. All dimensions are in mm.

term material property of the soft tissue and skin is assumed to be nonlinearly elastic, and the material parameters are obtained by fitting the constitutive Eq. (5) to the reported uniaxial experimental data [23]. The material parameters associated with the viscous deformation were obtained by fitting the stress relaxation Eq. (2) to the reported experimental data for human skin [23,29].

2.3. Numerical tests

Three series of numerical tests were performed in this study. The purpose of the first series of tests was to determine the material parameters of the soft tissue and to demonstrate the characteristics of the constitutive law used in the present simulations. The behaviour of the soft tissue defined using the proposed model is demonstrated in numerical tests of uniaxial tension/compression, confined compression, and constrained tension. In the tests of confined compression and constrained tension, the specimens are loaded (tension or compression) in one direction while the displacements in lateral directions are restricted. The second series of tests were performed to study the dynamic response of a fingertip to a prescribed displacement, which is varied as a linear function of time (ramp). The steel plate was displaced upwards by 3.0 mm within a ramping period of T_c and then downwards to the original position at the same rate (Fig. 2a). The reaction force of the fingertip was computed as a function of time for different ramping periods, T_c=1.0, 10.0, 50.0, and 100.0 s. In the third series of tests, the dynamic response of the fingertip to a prescribed sinusoidal vibration was investigated. The steel plate was first moved up by a displacement of 3.0 mm (T_c=1.0 s); and it was then kept at that position for a period of 10.0 s, to allow for the relaxation of the reaction force of the fingertip, which approached a quasi-steady state (Fig. 2b). The contacting steel plate was then subjected to sinusoidal motion with peak displacement of 0.5 mm at three discrete frequencies of 1, 10.0, and 31.5 Hz, to study the effects of loading frequency. Ten hertz is a typical dominant frequency of tampers, 31.5 Hz is a representative dominant frequency of the operations of paving breakers, jackhammers and chipping hammers [36], while the test at 1 Hz serves as a quasi-static reference. Fig. 2b shows the prescribed movement of the steel plate performed at a vibration frequency of 1 Hz. The analyses were carried out to derive the contact force and displacement within different tissue layers as a function of time, and the time-dependent distributions of strain and stress within the soft tissue.

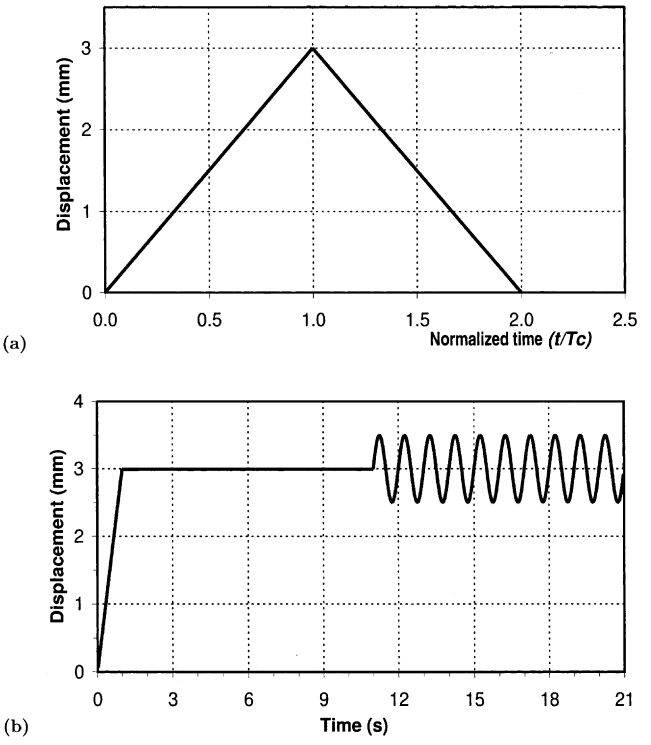

Fig. 2. Prescribed displacement of the steel plate: (a) Ramping displacement. Numerical tests were performed for four different ramping periods: T_c=1, 10, 50, and 100 s. (b) Sinusoidal vibration (the figure shows f=1 Hz). The steel plate was first moved upwards by 3.0 mm within a ramping period of 1 s, held constant for 10 s, and then subjected to sinusoidal vibrations with a vibration magnitude of 0.5 mm and frequencies of 1, 10 and 31.5 Hz.

3. Results

3.1. Parameter identification

The material parameters associated with strain energy function, described in Eq. (4), are identified by fitting Eq. (3) or (5) to the uniaxial tension tests for the human skin reported by Pan et al. [23]. The analysis performed by considering three terms (N=3) [Eq. (3)] resulted in a maximal error within 1% and the parameters, μ_i and α_i, were determined as: $\mu_i(i=1,2,3)=-0.07594$, 0.01138, and 0.06572; $\alpha_i(i=1,2,3)=4.941$, 6.425, and 4.712. A constant value of Poisson's ratio, ν=0.40, was assumed in the parameter identification. In a (nominal) strain range from −0.5 to +0.5, the soft tissue was assumed to exhibit symmetric behaviour in tension and compression in a nominal stress/strain scale (i.e. the stress and strain defined with reference to the original undeformed structure). The stress–strain curves derived from the proposed model were compared to the experimental data of human skin by Pan et al. (1998) and Dunn et al. (1985) [23,37] in a nominal stress/strain scale (Fig. 3a). The results show that the proposed constitutive model can fit well to the experimental data. In a scale of true stress (Cauchy stress) and logarithmic strain, however, the soft tissue

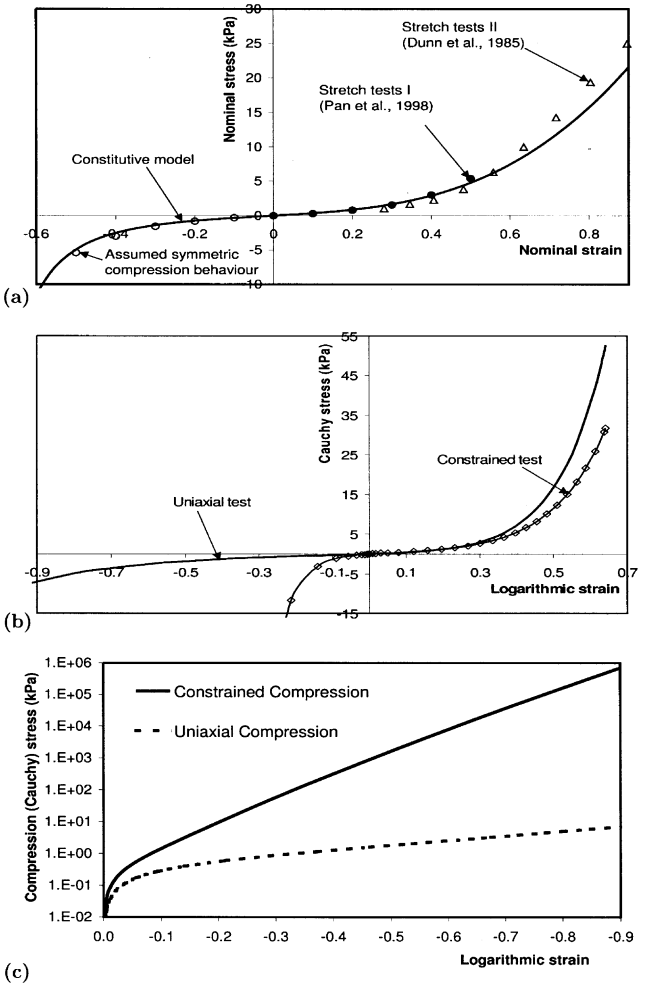

Fig. 3. Elastic deformation behaviour of the proposed constitutive model for the soft tissue. (a) In a nominal stress/strain scale (i.e. the stress and strain defined with reference to the original undeformed structure), the proposed soft tissue model [Eq. (5)] agree well with the experimental data of human skins reported by Pan et al. [23] and Dunn et al. [37]; the proposed model was assumed to be symmetric in uniaxial tension/compression in the nominal stress/strain scale (in a strain range of ±50%). (b) In a true stress/strain (Cauchy stress/logarithmic strain) scale, the proposed soft tissue model [Eq. (5)] is asymmetric in constrained and uniaxial tension/compression tests. (c) The stress/strain relations in compression [Fig. 3(b)] are re-plotted in a logarithmic scale and in a large stress range. The Material parameters for the elastic deformation were identified as: $\mu_i(i=1,2,3)=-0.07594$, 0.01138, and 0.06572; $\alpha_i(i=1,2,3)=4.941$, 6.425, and 4.712. A constant Poisson's ratio, $\nu=0.40$, was assumed in the curve fitting.

exhibits asymmetric properties in tension and compression under both uniaxial and constrained deformation, as shown in Fig. 3b. Since the soft tissues in fingertips are mostly under compression for biological loading conditions, the deformation behaviour of the soft tissue represented by the proposed model (Fig. 3b) is re-plotted in a logarithmic scale and in a large range of stress, as in Fig. 3c. A lateral constraint has a significant effect on the deformation in compression (Fig. 3c), while it has only little effect on the deformation in tension (Fig. 3b). Furthermore, the tissue exhibits considerably higher stiffness under the confined compression compared to that under constrained tension (Fig. 3b).

The material parameters in the stress relaxation function were determined by fitting Eq. (2) to the experimental data reported by Wan [29]. Based on the data reported in the literature [27,29,38], it was assumed that 40% of the initially applied load can be recovered in a stress relaxation test. Using a two-term Prony series [N=2, Eq. (2)], the maximal error in the curve-fitting can be kept within 1% and the material parameters were determined as: $g_i(i=1,2)=0.1480$ and 0.2520; and $\tau_i(i=1,2)=2.123$ and 9.371 s. The relaxation function used in the present study was compared with the reported data from typical stress relaxation tests of the human skin [29], porcine soft tissue (skin and subcutaneous) [28], and human ligament [39], as shown in Fig. 4.

3.2. Response of fingertip under ramping displacement

Finite element analyses were performed on the second series of tests using the identified material parameters to derive the contact force, the deformation in different tissue layers, and stress and strain fields under prescribed ramp and harmonic displacements. The contact forces of the fingertip as a function of the displacement for prescribed ramping displacements with different rates or ramping periods were predicted (Fig. 5). The predicted peak response force increases considerably with the increase of the ramping rate, consequently exhibiting the hysteretic properties of the soft tissue. The hysteretic or viscous effect is almost negligible under high-rate loading ($T_c<1.0$ s). The viscous effect becomes quite appar-

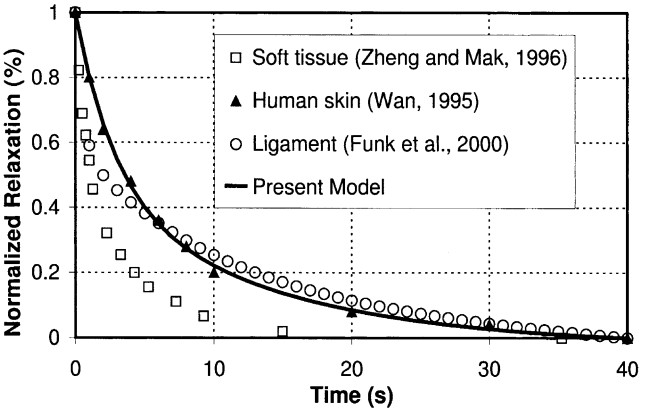

Fig. 4. Normalized stress relaxation curve of the proposed model describing viscoelastic deformation of the soft tissue. Two-term Prony series (Eq. (2)) were fitted to the experimental measurements of human skin [29]. The proposed model was compared to the relaxation behaviours of human ligament [39] and porcine soft tissue (skin and subcutaneous) [28]. The material parameters for the viscous deformation were determined as: $g_i(i=1,2)=0.1480$, 0.2520; $\tau_i(i=1,2)=2.123$ and 9.371 s. It is assumed that 40% of the initially applied force is recovered during the stress relaxation test.

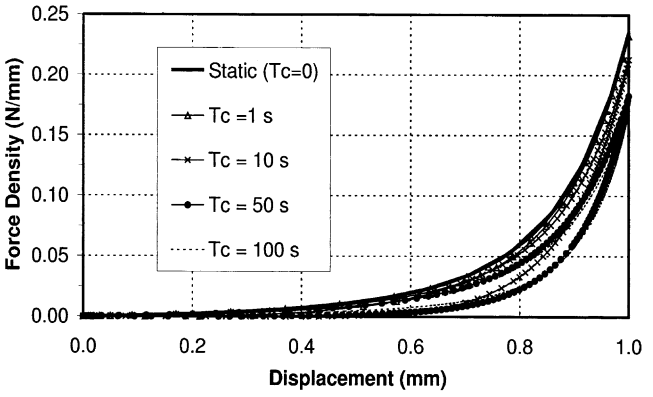

Fig. 5. Model prediction of the hysteric loading/unloading curves of a fingertip undergoing ramped displacement at different rates (the corresponding forcing function is shown in Fig. 2a). The contact force density as a function of displacement is plotted in the figure. The ramping period was varied from 0 to 100 s [i.e. T_c=0 (static), 1, 10, 50, and 100 s].

ent under a slow rate of loading (T_c>10 s). The results also show progressive hardening effect with increasing deformation, similar to that observed from the stress–strain curves presented in Fig. 3. The distributions of (logarithmic) strains in vertical and horizontal directions obtained from the test with prescribed ramping compression (T_c=1.0 s) are depicted in Fig. 6. At t=T_c=1.0 s, when the fingertip is compressed to the maximal displacement (3.0 mm), the tissue experiences a large deformation and the local (logarithmic) strain in the vertical direction, near the contact surface, approaches a value as large as −95% (Fig. 6b). The corresponding local tissue (logarithmic) strain in the horizontal direction reaches about 64% (Fig. 6a). The local strain of the tissue decreases as the depth from the contact surface increases. When the contacting plate returns to its original position, i.e. t=2T_c=2.0 s, there is still residual strain in the tissue (Fig. 6c and d). The fingertip tends to lose contact with the steel plate due to hysteresis or delayed deformation behaviour. This phenomenon can also be seen from the contact force–displacement curves (Fig. 5), where the contact force approaches zero corresponding to a non-zero displacement.

The maximal shear strain across the depth of the soft tissue under the prescribed ramp displacement of the contacting plate are evaluated to study the localized strain behaviour and its time-dependency. The distributions of the maximal shear (logarithmic) strain across the depth of the soft tissue for the two tests with different ramping periods (T_c=1.0 and 100 s) in loading and unloading stages are illustrated in Fig. 7a–d. It is seen that the peak of the maximal shear strain during the loading stage occurs at a depth of 2.0–3.0 mm from the contact surface, irrespective of the time and loading rate. The distribution of the maximal shear strain, however, is relatively uniform in a range of 1.0–4.0 mm from the contact surface. A comparison of the maximal shear (logarithmic) strain obtained in the tests with ramp periods T_c=1.0 and 100 s, as presented in Fig. 7a and c, suggest that the loading frequency has negligible effect on the strain distribution in the loading stage ($t \leq T_c$). The residual strain distribution across the soft tissue in the unloading stage (Fig. 7b and d), however, is affected considerably by the rate of loading/unloading. The residual strain obtained under a slow rate of loading/unloading (T_c=100 s) is considerably smaller than that obtained under a relatively fast rate of loading/unloading (T_c=1 s).

The distributions of von Mises stress across the depth of the fingertip soft tissue are also evaluated during loading and unloading stages (Fig. 8a–d). The peak stress in the loading stage for the test with fast loading rate (T_c=1 s, Fig. 8a) is approximately 40% higher compared to that with the slow loading rate (T_c=100 s, Fig. 8c). At a depth of approximately 3.0 mm from the skin surface, the magnitude of stress reaches a peak value. The stress is released almost completely for the test with slow loading rate (T_c=100 s, Fig. 8d) during unloading; while the faster rate of loading (T_c=1 s, Fig. 8b) yields a residual stress, approximately 5% of the peak stress magnitude, within the soft tissue.

3.3. Response of fingertip under cyclic displacement

The third group of tests were performed to investigate the responses of the fingertip to cyclic loading. The fingertip is subjected to a pre-load by displacing the contacting plate upwards by 3.0 mm within a ramp period of 1.0 s (Fig. 2). The position of the steel plate is then held constant for 10 s, where the corresponding contact force allowed to relax and approach a nearly steady-state value (results not shown), approximately 0.18 N/mm. Assuming an average section thickness of 10 mm in the proposed two-dimensional model, the initial contact force between the fingertip and the plate is approximately 1.8 N, which is within the range of the grip force studied by Gurram et al. [40]. The contact plate is then subjected to a sinusoidal motion with an amplitude of 0.5 mm for ten cycles. The displacements at different depths from the skin surface (at 0.00, 0.53, 1.21, 2.13, and 3.35 mm, measured from the contact surface of the undeformed fingertip) and nail, as well as the resultant contact force were predicted as a function of time for three different cycling frequencies (the results for f=1 and 10 Hz are shown in Figs. 9 and 10, respectively). The frequency of the oscillatory deformation at different layers in the soft tissue are identical to those of the prescribed motion, while the phase response is negligible at such low frequencies. The time-histories of contact force and displacement for the first ten cycles of the test at 31.5 Hz are similar to that at 10 Hz (results not shown).

The contact force approaches zero during the

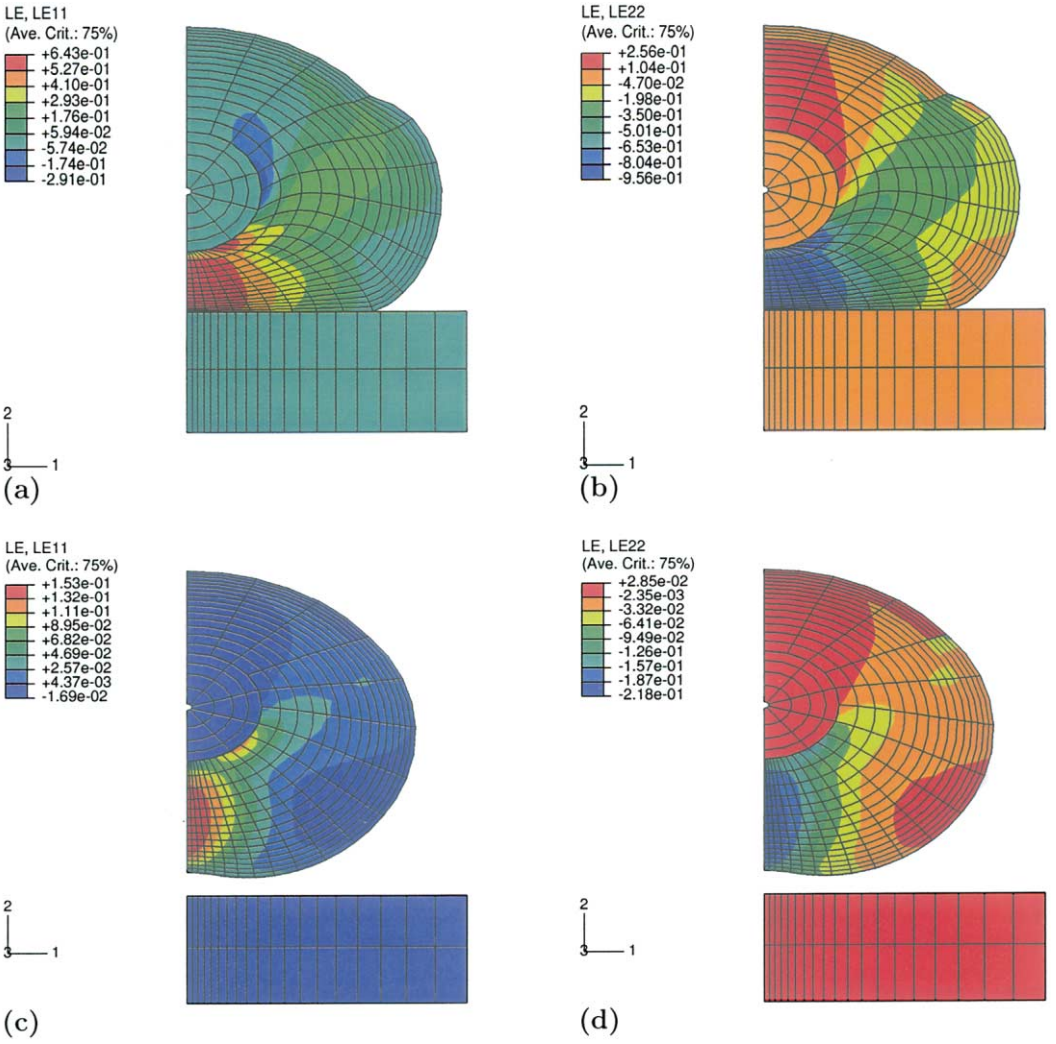

Fig. 6. Predicted distributions of the (logarithmic) strain in the fingertip at the maximal compressed [(a),(b), $t=T_c$] and the unloaded state [(c),(d), $t=2T_c$] for the test with the ramping period $T_c=1$ s. (a) Horizontal (logarithmic) strain at $t=T_c$; (b) Vertical (logarithmic) strain at $t=T_c$; (c) Horizontal (logarithmic) strain at $t=2T_c$; (d) Vertical (logarithmic) strain at $t=2T_c$.

unloading portion of the displacement cycle for both excitation frequencies (Figs. 9 and 10), indicating a loss of contact between the fingertip and the steel plate. The ratio of the separation duration over the total cycling period increases with the increasing cycling number (i.e. increasing the duration of cycling) and reaches a steady-state value after a sufficient long cycling period.

The distributions of the strain and stress across the soft tissue vary as a function of time and approach to a steady-state after a sufficient long period of cycling time. Fig. 11 shows the steady-state distributions of the cycling deformation and stress across the soft tissue in the fingertip. The magnitude of the cycling displacement of the soft tissue is linearly distributed across the thickness of the tissue (Fig. 11a); it reaches the maximum near the contact surface and zero near the bone–tissue interface. The von Mises stress is nonlinearly distributed across the finger tissue; it reaches a peak at a depth around 2.0 mm. In the range of depth from 1.0 to 3.0 mm, the variation of von Mises stress is small. The results suggest that the excitation at higher frequency (31.5 Hz) induces higher deformation (Fig. 11a) and higher stress (Fig. 11b) in the tissue compared to the excitation at lower frequency (1 Hz).

4. Discussion and conclusion

Grasping a tool handle with a specified grip force, in general, yields a high concentration of interface pressure at the tips of index, middle, and ring fingers. It has been shown that a handle grip of 25 N yields a pressure of approximately 80 kPa at the tip of the index finger [7]. These results suggest excessive loading of the skin, soft tissues, and arterial walls near the fingertips. It has been speculated that the high local contact pressure under tool vibration affects the arterial blood flow, and could induce the degeneration of the vascular systems, and

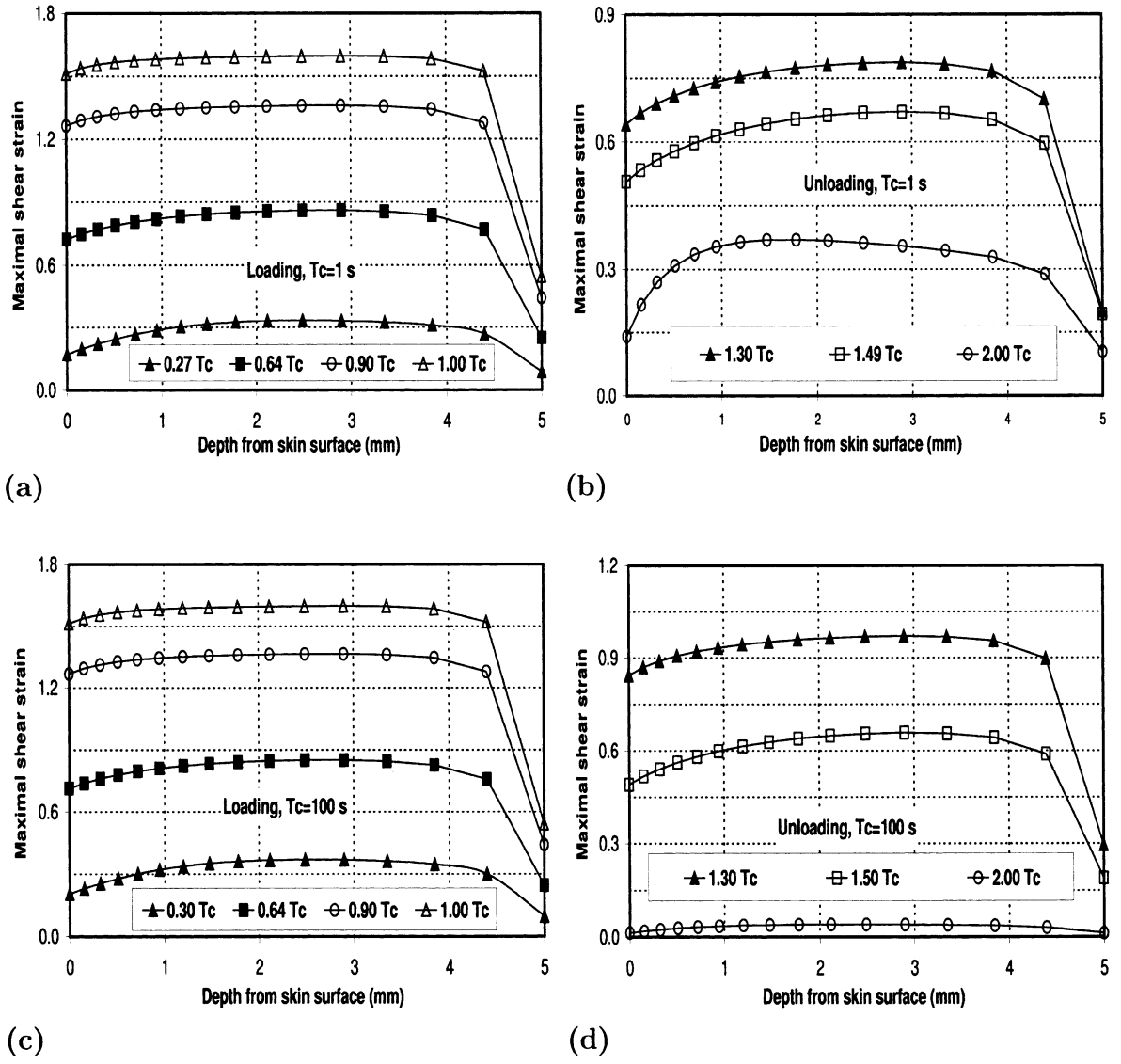

Fig. 7. Predicted distributions of the maximal shear (logarithmic) strain across the soft tissue (at the central line of the fingertip) as a function of time. (a) Loading period for the test with T_c=1 s; (b) Unloading period for the test with T_c=1 s; (c) Loading period for the test with T_c=100 s; (d) Unloading period for the test with T_c=100 s.

finally, lead to the development of VWF [11]. In order to understand the mechanism of development of VWF and other vibration-induced musculoskeletal diseases, it is important to know the time-dependent stress and strain fields within the soft tissue in a vibration environment. The dynamic time-dependent stress and strain distributions within the soft tissue under vibration, however, have not yet been characterized experimentally or theoretically due to technical complexities. A model based upon a simplified in-plane representation of the fingertip incorporating time-dependent properties of the soft tissues could thus provide considerable insight into the tissue response under localized static and dynamic loading that may occur while operating a hand-held power tool. The purpose of the present research is to develop a model to analyze the time-dependent stress and strain distributions within the tissue in a vibrating environment, and the mechanical responses of a fingertip to dynamic loading.

Our simulations suggest that the deformation of the fingertip under dynamic loading is time-dependent. The current deformation state of the tissue depends not only on the current loading but also on the loading in the deformation history. Therefore, for the tests under prescribed displacement of the contacting plate, the fingertip may lose contact with the contact surface during the unloading phase. The length of the period of the separation between the fingertip and the contacting surface is associated with the loading rate or vibration frequency. The duration of the tissue recovery depends on the rate of loading. This phenomenon has been reported by Gurram et al. [20], who observed that the local contact press-

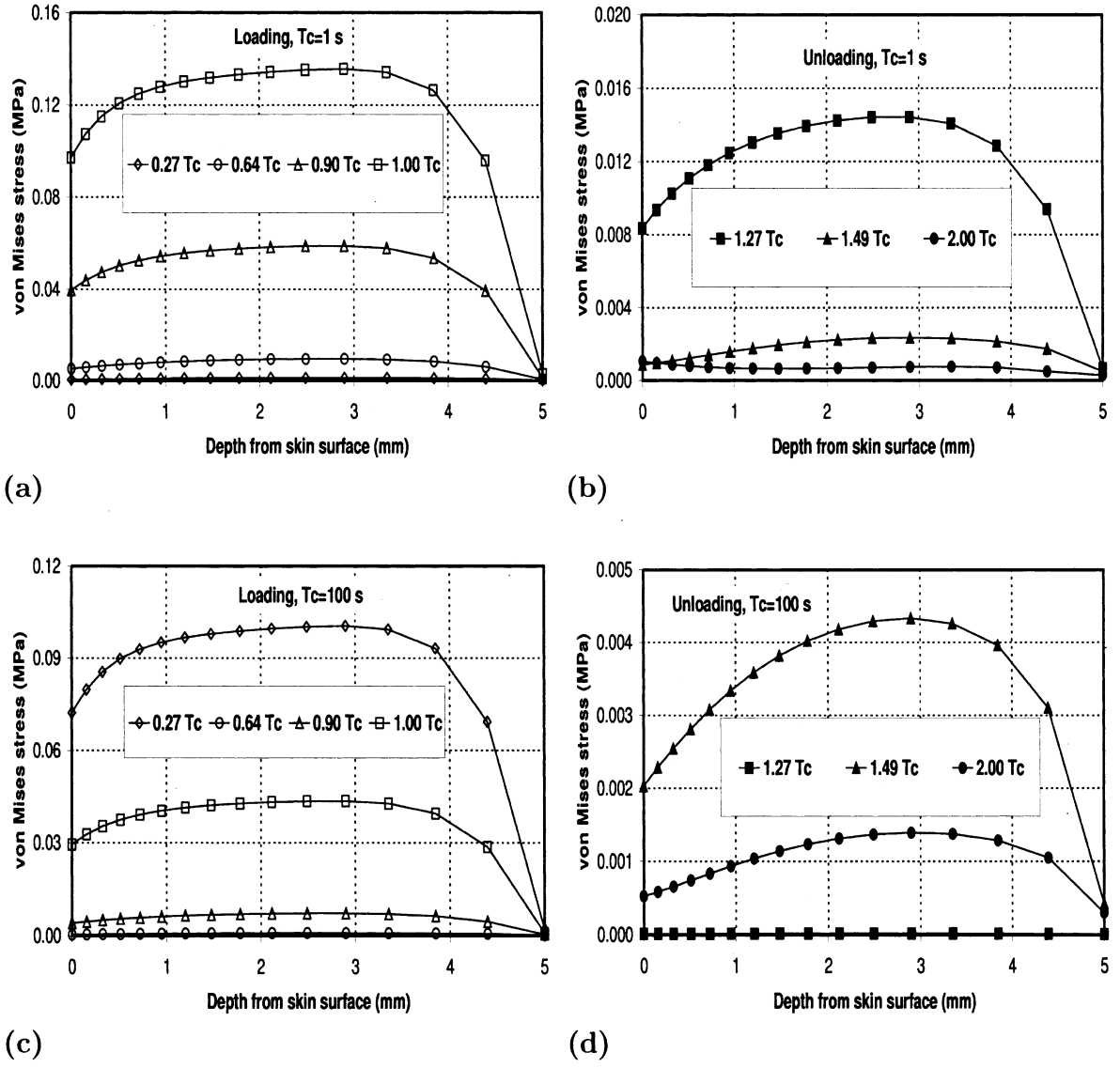

Fig. 8. Predicted distributions of von Mises stress across the soft tissue (at the central line of the fingertip) as a function of time. (a) Loading period for the test with T_c=1 s; (b) Unloading period for the test with T_c=1 s; (c) Loading period for the test with T_c=100 s; (d) Unloading period for the test with T_c=100 s.

ure between the fingers and the handle of a vibrating hand-tool was reduced to zero at certain frequencies. The dependence of the separation ratio on the cycling frequency however, was not examined in the reported study.

The constitutive equation for the soft tissue used in the present study was calibrated using the test results obtained for skin in tension [23]. Our constitutive equation for skin is qualitatively comparable with the loading/displacement curves by Wan [29], however, a quantitative calibration cannot be carried out using Wan's data because the thickness of the skin specimen was not available.

The bone and nail were assumed to have a Poisson's ratio of 0.30, which is typical for most linear-elastic materials undergoing small deformation. A constant value of Poisson's ratio (ν=0.40) of the soft tissue was assumed in our analysis, implying that the compressibility of the soft tissue is assumed to lie between that of hard tissue (e.g. bone, ν=0.3) and incompressible fluid (ν=0.5). The soft tissue of a fingertip remains mostly in compression under vibratory loading. However, almost all experimental data for skin and soft tissues available in literature were obtained in tensile tests. Poisson's ratio for soft tissues has not yet been studied systematically. The compressibility of the soft tissue may be strain-dependent, which means that Poisson's ratio may not be constant. Further efforts are thus needed to calibrate the constitutive model of the soft tissue under uniaxial and confined compression/tension tests, where ν should be obtained as a function of the deformation.

The model prediction on the force response agrees

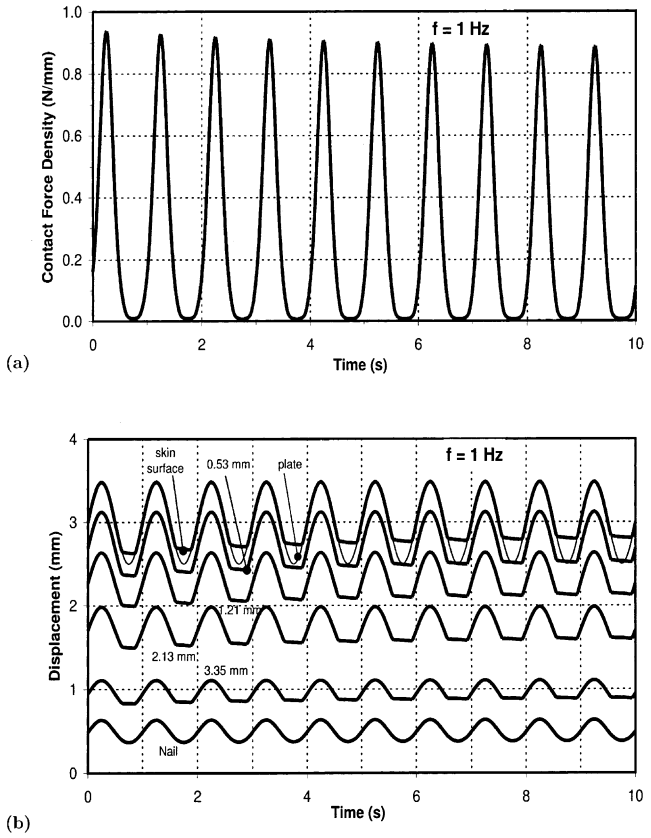

Fig. 9. Predicted contact force and displacements at different locations within the fingertip as a function of time (f=1 Hz). (a) Contact force density of the fingertip as a function of time; (b) Time-history of the displacements at the contacting plate, the nail, the skin surface, and in the depths of 0.53, 1.21, 2.13, and 3.35 mm from the skin surface (measured at the undeformed state and in the central line of the fingertip).

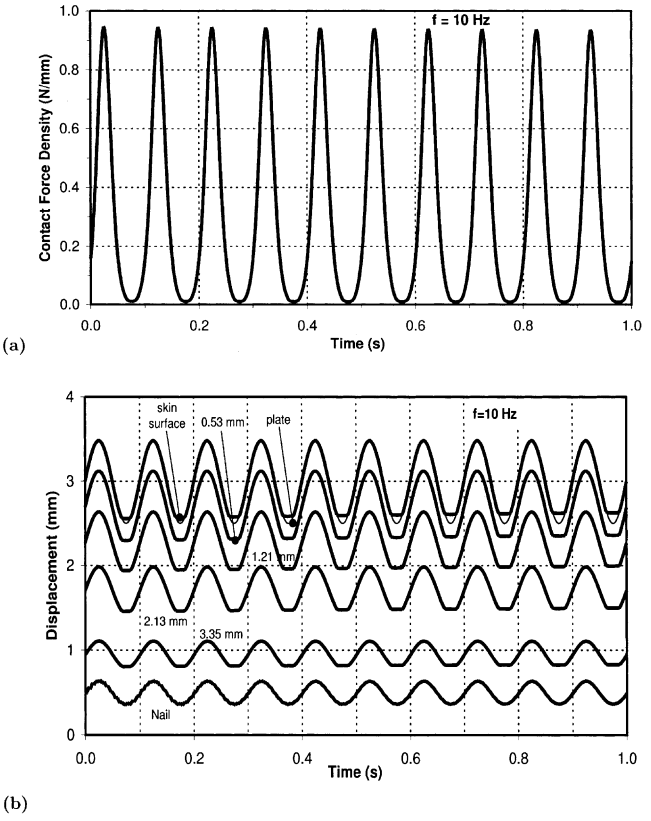

Fig. 10. Predicted contact force and displacements at different locations within the fingertip as a function of time (f=10 Hz). (a) Contact force density of the fingertip as a function of time; (b) Time-history of the displacements at the contacting plate, the nail, the skin surface, and in the depths of 0.53, 1.21, 2.13, and 3.35 mm from the skin surface (measured at the undeformed state and in the central line of the fingertip).

qualitatively with the experimental results (pulp force–displacement relationship) by Serina et al. [41]. However, a qualitative comparison cannot be made because of the difference between the finite element model and the experimental configuration [41].

In our finite element model, the bone is assumed to be fixed to realize the compression of the soft tissue. Under exposure to vibration, the arterial bone encounters low magnitude motions mostly associated with the rigid-body mode. The rigid-body motion of the bone could contribute to the resulting stress/strain fields of the soft tissue due to the inertia force associated with the bone and the variations in the compressive deformation of the soft tissue, induced by the relative displacement between the bone and the contacting plate (Fig. 1). The effects of the inertia force, however, is considered to be negligible in the frequency range investigated in the present study. The effects of the variations in the compressive deformation of the soft tissue, on the other hand, are effectively investigated by varying the magnitude of the prescribed vibration.

In the present simulations, the fingertip has been assumed to be directly in contact with the vibrating plate. The simulations are representative for the practical case of grasping a power tool using a bare hand. We have observed, in our recent field studies, that the wrapping materials on the handles were often worn out. Gloves were also worn out in some scenarios, resulting in a nearly 'bare contact' between the finger and the handle of the power tool. The effects of glove and wrapping materials on the dynamic interaction between finger and power tool can be studied using the proposed methodology; it is, however, beyond the scope of the present study.

Due to the lack of adequate knowledge of the time-dependent properties of the biological material and technical complexities associated with modeling of the fingertip tissue in a dynamic loading environment, the soft tissue of the fingertip is assumed to be uniform and isotropic. This simplified model is considered to yield considerable insight into stress and deformation fields of the tissue under oscillatory loads. It is known that physiological soft tissue contains many anatomical substructures, e.g. tendons, vessels, and other non-uniform

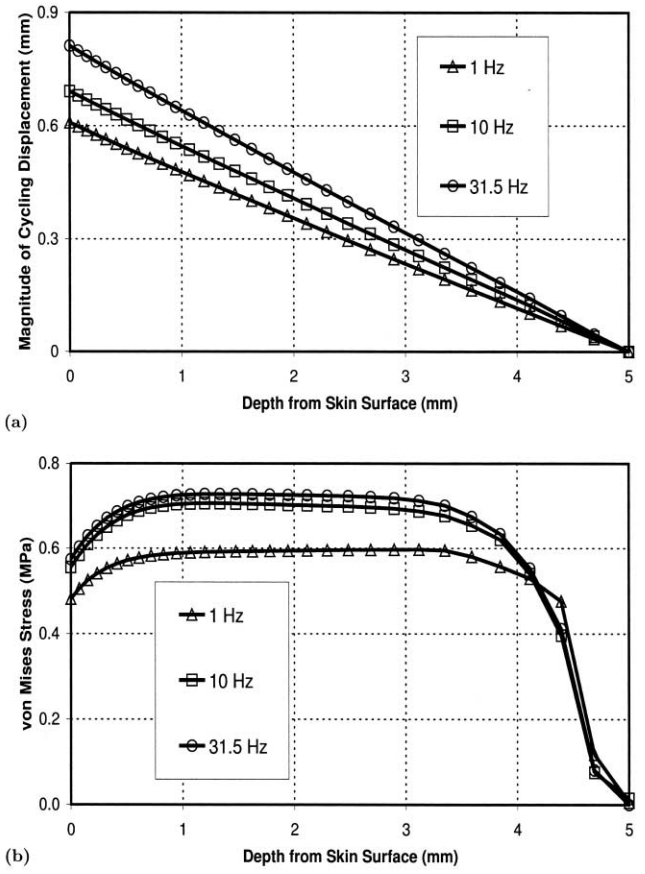

Fig. 11. Predicted steady-state distributions of the magnitude of the cycling displacement and von Mises stress across the soft tissue (at the central line of the fingertip) for the tests with frequencies of 1, 10, and 31.5 Hz. (a) The distributions of the magnitude of cycling displacement; (b) The distributions of von Mises stress.

connective tissues. Consequently, physiological soft tissue exhibits non-uniform and heterogeneous properties. The calibration of the constitutive equation proposed in this study, when performed using a real soft tissue containing all these anatomical substructures, could be effectively applied to study the effects of non-uniformity of the soft tissue.

In the present study, the numerical simulations of the dynamic responses of the fingertip under vibration were performed under a specified preload. The static preload and vibratory motion at the contact surface represents the interactions between the hand and a power tool. A few studies investigated the relationship between the magnitude of the grip force associated with grasping a tool handle affects the nature of hand transmitted vibration and the vibration response of the human hand–arm system expressed in terms of driving-point mechanical impedence [40]. The effects of grip force on the mechanical response of the fingertip in vibration have not yet been investigated.

A two-dimensional finite element model was developed herein to study the interaction between the fingertip and a vibration surface. Unlike previous mechanical-equivalent hand–arm vibration models, the proposed model is developed on the basis of the physical properties of the soft tissue and the anatomical structures of the fingertip, and is capable of predicting the time-dependent stress/strain distributions within the soft tissues under static and dynamic loading. To the best of the authors' knowledge, the proposed model represents the first 'biodynamic' model which simulates the *dynamic* responses of the *biological* tissues under a vibratory environment. The results of the present study suggest that the fingertip may separate from the contact surface subjected to sinusoidal vibration, where the duration of the separation within a cycle depends on the rate of loading. The prescribed vibratory motion at a higher frequency yields higher stresses in the tissues when compared to those observed under a lower frequency vibration. The predicted time-dependent deformation fields in the soft tissue of fingertip under vibration environment can be used as the boundary conditions to simulate the effects of vibration on the local blood circulation. The present model could serve as a useful tool to study the mechanism of tissue degeneration under vibratory loading encountered during operation of hand-held power tools.

References

[1] Bernard B, Nelson N, Estill CF, Fine L. The NIOSH review of hand-arm vibration syndrome: vigilance is crutial. national istitute of occupational safety and health [editorial]. J Occup Environ Med 1998;40(9):780–5.
[2] Rawlinson D. Hand-arm vibration syndrome. In: The safety and health practitioner. 1990;8:11–15.
[3] Pelmear PL, Leong D. Review of occupational standards and guidelines for hand-arm (segmental) vibration syndrome (havs). Appl Occup Environ Hyg 2000;15(3):291–302.
[4] Bovenzi M. Digital arterial responsiveness to cold in healthy men, vibration white finger and primary Raynaud's phenomenon. Scand J Work, Environ Health 1993;19(4):271–6.
[5] Gemne G., Pyykko I. Finger blood flow and pressure in chainsawyers with a past history of vibration induced Raynaud's phenomenon. Technical report, Institut National de Recherche et de Securite, 1998.
[6] ISO-10068. International standard: Mechanical vibration and shock-free, mechanical impedance of the human hand-arm system at the driving point. Technical report, The International Organization For Standardization, 1998.
[7] Gurram R, Rakheja S, Gouw G. A study of hand grip pressure distribution and emg of finger flexor muscles under dynamic loads. Ergonomics 1995;38:684–99.
[8] ISO-8727. International standard: Mechanical vibration and shock—human exposure—biodynamic coordinate systems. Technical report. The International Organization For Standardization, 1997.
[9] Jahn R, Hesse M. Applications of hand-arm models in the investigation of the interaction between man and machine. Scand J Work, Environ Health 1986;12:343–6.
[10] Cherian T, Rakheja S, Bhat RB. An analytical investigation of an energy flow divider to attenuate hand-transmitted vibration. Int J Ind Ergonomics 1996;17:455–67.

[11] Bovenzi M. Vibration-induced white finger and cold response of digital arterial vessels in occupational groups with various patterns of exposure to hand-transmitted vibration. Scand J Work, Environ Health 1998;24(2):138–44.
[12] Dimberg L, Oden A. White finger symptoms: a cross-sectional study. Aviat Space Environ Med 1991;62(9 Pt 1):879–83.
[13] Taylor W, Ogston S, Brammer A. A clinical assessment of seventy-eight cases of hand-arm vibration syndrome. Scand J Work, Environ Health 1986;12:265–8.
[14] Pyykko I, Kolari K, Farkkila M, Starck J, Korhonen D, Jantti V. Finger peripheral resistance during local cold provocation in vasospastic disease. Scand J Work, Environ Health 1986;12:395–9.
[15] Nerem RM. Vibration enhancement of blood-arterial wall macromolecule transport. In: Proc. of the Int. Hand-Arm Vibration Conf. 1977.
[16] Bovenzi M. Vibration white finger, digital blood pressure, and some biochemical findings on workers operating vibrating tools in the engine manufacturing industry. Am J Ind Med 1988;14(5):575–84.
[17] Ekenvall L, Lindblad LE. Vibration white finger and digital systolic pressure during cooling. Br J Ind Med 1986;43(4):280–3.
[18] Brubaker R, Mackenzie CJG, Hutton S. Vibration-induced white finger among selected underground rock drillers in British Columbia. Scand J Work, Environ Health 1986;12:296–300.
[19] Hellström B, Andersen KL. Vibration injuries in Norwegian forest workers. Br J Ind Med 1972;29(3):255–63.
[20] Gurram R, Rakheja S, Brammer AJ. Driving-point mechanical impedence of the human hand-arm: synthesis and model development. J Sound Vib 1995;180:437–58.
[21] Clark JA, Cheng JC, Leung KS. Mechanical properties of normal skin and hypertropic scars. Burns 1996;22(6):443–6.
[22] Edwards C, Marks R. Evaluation of biomechanical properties of human skin. Clin Dermatol 1995;13(4):375–80.
[23] Pan L, Zan L, Foster FS. Ultrasonic and viscoelastic properties of skin under transverse mechanical stress in vitro. Ultrasound Med Biol 1998;24(7):997–1007.
[24] Wan AW. Biaxal tension test of human skin in vivo. Biomed Mater Eng 1994;4(7):473–86.
[25] Wilhelmi BJ, Blackwell SJ, Mancoll JS, Phillips LG. Creep vs. stretch: a review of the viscoelastic properties of skin. Ann Plast Surg 1998;41(2):215–9.
[26] Dobrev H. In vivo study of skin mechanical properties in scleredema of buschke. Acta Derm Venereol 1998;78(2):103–6.
[27] Rubin MB, Bodner SR, Binur NS. An elastic-viscoplastic model for excised facial tissues. J Biomech Eng 1998;120(5):689–.
[28] Zheng YP, Mak AF. An ultrasound indentation system for biochemical properties assessment of soft tissues in-vivo. IEEE Trans Biomed Eng 1996;43(9):912–8.
[29] Wan AW. Stress stabilisation behaviours in skin under small tensile loads in vitro. Biomed Mater Eng 1995;5(2):59–63.
[30] HKS. *ABAQUS* theory mannual (version 5.8). Pawtucket, USA: Hibbitt, Karlsson and Sorensen, 1998.
[31] Tschoegl NW. The phenomenological theory of linear viscoelastic behavior: An introduction. New York: Springer-Verlag, 1989.
[32] Fung YC. Inversion of a class of nonlinear stress-strain relations of biological soft tissues. ASME J Biomech Eng 1979;101:23–7.
[33] Storakers B. On material representation and constitutive branching in finite conpressible elasticity. J Mech Phys Solid 1986;34(2):125–45.
[34] Clemente CD. Anatomy: A regional atlas of the human body., 2nd edn Baltimore-Munich: Urban and Achwarzengerg, 1981.
[35] Yamasa H. Strength of biological materials. Baltimore: Wiliams and Wilkins, 1970.
[36] Griffin M.J. Handbook of human vibration. Technical report, human Factors Research Unit, Institute of Sound and Vibration Research, 1990.
[37] Dunn MG, Silver FH, Swann DA. Mechanical analysis of hypertropic scar tissue: structural basis for apparent increased rigidity. J Invest Dermatol 1985;84:9–13.
[38] Barbenel JC, Evans JH. The time-dependent mechanical properties of skin. J Invest Dermatol 1977;69(3):318–20.
[39] Funk JR, Hall GW, Crandall JR, Pilkey WD. Linear and quasi-linear viscoelastic characterization of ankle ligaments. J Biomech Eng 2000;122(1):15–22.
[40] Gurram R, Rakheja S, Boileau PE, Gouw GJ. Development of a grip force dependent hand-arm vibration model. Cent Eur J Public Health 1996;4(1):65–8.
[41] Serina E.R., Mote C.D., Rempel D. Force response of the fingertip pulp to repeated compression-effects of loading rate, loading angle and anthropometry. J Biomech, 30(10):1035-40.